

A *CHANDRA* OBSERVATION OF THE TW HYDRAE ASSOCIATION BROWN DWARF 2MASSW J1139511-315921

Philip J. Castro¹ and John E. Gizis¹

Department of Physics and Astronomy, University of Delaware, Newark, DE 19716;
pcastro@udel.edu, gizis@udel.edu

Marc Gagné²

Department of Geology and Astronomy, West Chester University, West Chester, PA 19383;
mgagne@wcupa.edu

ABSTRACT

We report on a sequence of *Chandra* X-ray Observatory observations of the TW Hydrae brown dwarf (BD) 2MASSW J1139511-315921 (2M1139). In the combined 31 ks ACIS-S exposure, 2M1139 is detected at the 3σ confidence level. We find an X-ray luminosity of $L_X = 1.4_{-1.0}^{+2.7} \times 10^{26}$ ergs s⁻¹ or $\log L_X/L_{\text{bol}} = -4.8 \pm 0.3$. This object is similar to another TW Hydrae BD member, CD-33 7795B (TWA 5B): both have H α emission, both show no signatures of accretion, and both have comparable ages and spectral types. TWA 5B was previously detected in X-rays with a luminosity of $L_X = 4 \times 10^{27}$ ergs s⁻¹ or $\log L_X/L_{\text{bol}} = -3.4$, an order of magnitude more luminous in X-rays than 2M1139. We find that the discrepancy between the X-ray luminosity of 2M1139 and TWA 5B is consistent with the spread in X-ray luminosity in the Orion Nebula Cluster (ONC) for BDs of similar spectral types. Though rotation may play a role in the X-ray activity of ultracool dwarfs like 2M1139 and TWA 5B, the discrepancy cannot be explained by rotation alone. We also examine two X-ray bright objects in the FOV of our *Chandra* observations and find one to be of spectral type K0IV and identify it as a possible RS Canum Venaticorum (RS CVn), and another X-ray bright object whose light-curve clearly shows the decay phase of an X-ray flare.

Subject headings: brown dwarfs - open clusters and associations: individual (TW Hydrae) - stars: activity - stars: coronae - X-rays: stars

1. INTRODUCTION

Brown dwarfs are objects whose mass is too low to sustain hydrogen fusion, but massive enough to fuse deuterium. With M in the range $0.01 - 0.075M_{\odot}$, brown dwarfs lay in the mass gap between stars and planets. Objects in this mass range are fully convective, like all stars below $0.35M_{\odot}$ (Chabrier & Baraffe 1997). Solar mass stars generate large-scale magnetic fields by amplifying the small-scale fields at the boundary layer (the tachocline) of the radiation zone and the convective envelope via differential rotation. The $\alpha - \Omega$ dynamo mechanism was first proposed by Parker (1955) and its general features have been confirmed by helioseismology (Charbonneau 2010). Some fully convective objects are known to have strong chromospheric $H\alpha$ emission, which is a signature of magnetic activity (Browning 2008). Since fully convective objects, low mass stars and brown dwarfs, don't have a boundary layer to generate large-scale magnetic fields like their more massive counterparts through the $\alpha - \Omega$ dynamo, there must be some other mechanism responsible for the generation of magnetic fields in these objects. A turbulent dynamo which creates small-scale magnetic fields has been suggested by Durney et al. (1993), where other mechanisms that create large-scale magnetic fields have been suggested such as the α^2 and $\alpha^2 - \Omega$ dynamo (Chabrier & Küker 2006).

The first X-ray detection of a brown dwarf was Cha $H\alpha$ 1 by Neuhauser & Comeron (1998), who suggested that the quiescent X-ray emission was a result of a magnetically supported corona. Since then BDs have been studied and detected in X-rays, field BDs such as LP 944-20; (Rutledge et al. 2000), Gl 569 Bab; (Stelzer 2004), and BDs in various star forming regions: ONC; (Feigelson et al. 2002; Preibisch et al. 2005b), Taurus; (Grosso et al. 2007), Chamaeleon; (Neuhäuser et al. 1999), Pleiades; (Briggs & Pye 2004), Rho Ophiucus; (Imanishi et al. 2001; Gagné et al. 2004), IC 348; (Preibisch & Zinnecker 2002), and TWA 5B; (Tsuboi et al. 2003). Many mid to late substellar M dwarfs have observed $H\alpha$ emission. $H\alpha$ is indicative of chromospheric activity and accretion, with a steep drop at M9 and later (Mohanty & Basri 2003; Gizis et al. 2000). It has been proposed that the chromosphere is heated by the overlying corona (indicated by X-ray emission) (Preibisch & Zinnecker 2002; Fleming et al. 1988). This results in a physical relation between the chromosphere and the corona (Tsuboi et al. 2003; Gizis & Bharat 2004; Cram 1982). During this time a puzzling picture has emerged for X-ray emission from BDs, with some BDs being detected in X-rays and others not.

The TW Hydrae association has four confirmed BDs: 2MASSW J1207334-393254 (2M1207), 2MASSW J1139511-315921 (2M1139), CD-33 7795B (TWA 5B), and SSSPM J1102-3431 (SSSPM 1102). The M8 BD 2M1139, and the M8 BD 2M1207, were discovered by Gizis (2002) during a survey of the TW Hydrae association in search of BDs. TWA 5B, an

M8.5 BD, was discovered as a companion to TWA 5A at a distance of approximately $2''$ by Lowrance et al. (1999) using the NIMCOS coronagraph on the Hubble Space Telescope (HST). SSSPM 1102, an M8.5 BD, was discovered by Scholz et al. (2005b). DENIS J124514.1-442907 (DENIS 1245) is the fifth substellar member within the line of sight of TW Hydrae but has yet to be confirmed by astrometry as a member of the association (Looper et al. 2007). This association is an ideal place to study BDs and their X-ray emission, with its close proximity of ~ 50 pc (Mamajek 2005), an age of $\sim 8 - 10$ Myr (Song et al. 2003; Webb et al. 1999), and a small sample of well studied bona fide BDs. These four confirmed BDs are about the same age, and have comparable spectral types, all ranging within half a spectral subtype of M8.5. They provide a laboratory to study X-ray emission from BDs with the variables of mass, age, and spectral type (effective temperature) as a control.

This paper reports on the X-ray observations of the bona fide BD of TW Hydrae, 2M1139, providing all of the confirmed BDs in TW Hydrae with either an X-ray detection or an upper limit. We will first discuss the observations, source detection, and astrometry (section 2), our discussion (section 3), and finally our conclusions (section 4). In the appendix we provide a brief discussion of two X-ray bright objects in the FOV of our *Chandra* observations.

2. OBSERVATIONS AND CIAO DATA REDUCTION

2.1. *Chandra* Observations

Chandra observed 2M1139 in a sequence of three observations in cycle 9, sequence number 200494. The first observation, *Chandra* observation ID (ObsId) 9835, was observed on 2008 March 13th at 14:32 UT until 17:14 UT, having a live-time on CCD 7 of 8.0 ks (2.2 hrs). The second observation, *Chandra* ObsId 8913, was observed on 2008 March 17th at 6:01 UT until 8:19 UT, having a live-time on CCD 7 of 7.1 ks (2.0 hrs). The third observation, *Chandra* ObsId 9841, was observed on 2008 August 19th at 1:40 UT until 6:35 UT, having a live-time on CCD 7 of 15.8 ks (4.4 hrs). The roll angle of ObsId 9841 differs from the common roll angle of the other ObsIds by -145° , and the aim point is offset from the common aim point of the other ObsIds by $\sim 0.5'$. All three observations were obtained in ‘faint’ format, and ‘timed exposure’ mode, with a time resolution of 3.2 s using the Advanced CCD Imaging Spectrometer (ACIS) with chips S1-S4, and I2-I3 enabled. The target falls on chip S3 so our discussion will only refer to this chip. Chip S3 is a back-illuminated CCD with dimensions 1024 x 1024 pixels, spanning a FOV of $8' \times 8'$, with a pixel size of $24.0 \mu\text{m}$ with a spatial resolution at aim point of $0''.492 \pm 0''.0001$. The back-illuminated S3 chip is better for detecting low energy sources than its front-illuminated counterpart (Weisskopf et al. 2002),

I0-I3, this is due to its larger effective area at lower energies (higher sensitivity). Further details regarding *Chandra* can be found in the *Chandra* Proposers' Observatory Guide¹.

2.2. CIAO Data Reduction

We applied the standard data reduction pipeline using CIAO software version 4.0.2. `Acis_process_events` was run on each ObsId evt1 fits file. 1) Pixel randomization was removed, 2) Filtered for bad grades and a clean status column, grades=0,2,3,4,6 with a status=0 were kept, 3) Good Time Interval's were applied (GTI) which resulted in an evt2 fits file. Finally, the energy was filtered from 0.1-8 keV keeping in line with Tsuboi et al. (2003).

2.3. Image Creation and Source Detection

All three observations of sequence 200494, ObsId 9835, ObsId 8913, and ObsId 9841, were merged using the CIAO routine `MERGE_ALL`. An image of the merged observations was created with dimensions 1950 x 1600 pixels. `WAVDETECT` was run on the image with scales 1, 2, 4, 8, and 16, and with a significance threshold of 5×10^{-7} . Given that the merged observations have an area of approximately 2×10^6 pixels² this should yield one false detection over the entire image. `WAVDETECT` yielded 25 source detections over the entire image, a cutoff of 1 net counts was made and one source was eliminated. 2M1139 was not detected in the full band image.

ACIS counts in the energy bands (0.1-1.5 keV), (1.5-2.5 keV), and (2.5-8 keV) were used to create RGB images. `WAVDETECT` was run on these images with the same scales and significance threshold as before. `WAVDETECT` detects a source in the soft band image, 0.1-1.5 keV, at (J2000) R.A. = $11^h39^m51^s.081$, Decl. = $-31^\circ59'21''.75$, $\sim 0''.25$ from the position of 2M1139 (as discussed in section 2.5), albeit with a 1D region due to the small number of counts combined with the spatial distribution of the photons. 2M1139 was not detected in the medium or hard images. The 3 counts from 2M1139 are from ObsId 9841 only. In order to assess the reliability of the `WAVDETECT` 2M1139 soft band detection, `Acis Extract (AE)` was applied to the observations.

¹Available at <http://cxc.harvard.edu>.

2.4. ACIS Extract

ACIS Extract (AE), a software package from Penn State (Broos et al. 2010), was used to perform an optimal source and background extraction, while accounting for the *Chandra* point spread function (PSF). ACIS Extract was run on the 3 ObsIds after the CIAO data reduction was completed. AE only used ObsId 9841 for 2M1139 due to the 3 photons being present only in this ObsId. AE found a detection with net counts of $2.84^{+2.94}_{-1.63}$ in the full band (0.5-8 keV), and net counts of $2.95^{+2.94}_{-1.63}$ in the soft band (0.5-2 keV), where the errors are 1σ upper and lower values. AE determined a ‘prob_no_source’ for the sources in the observations, ‘prob_no_source’ is a statistical measurement of the probability that a source could be a Poisson fluctuation in the background, and provides a classic confidence level. In the full band, a ‘prob_no_source’ of 6.3×10^{-4} was found for the null hypothesis, this yields a detection at the 3σ confidence level. For the soft band, a ‘prob_no_source’ of 1.9×10^{-5} was found for the null hypothesis, this yields a detection at the 4σ confidence level. The statistics in the soft band are more robust since all 3 photons are in this energy range and the background is reduced considerably in this energy band. With 3 photons it is not possible to determine whether this detection of X-ray emission is variable. Considering that the two shorter observations with no photons for 2M1139, ObsId 9835 and ObsId 8913, have exposure times that are approximately the spacing in photon arrival times from ObsId 9841, ~ 5 ks and ~ 7 ks, variability shouldn’t be assumed for ObsId 9841. *We conclude that we have a 3σ detection of X-ray emission at the location of 2M1139.*

2.5. Astrometry

We performed astrometry on the *Chandra* observations using an I-band image whose coordinate system was calibrated using the 2MASS catalog. The 2MASS catalog contained too few counterparts to *Chandra* sources to confidently perform astrometry directly using the 2MASS catalog.

2M1139 was observed in the I-band on March 24, 2007 with an exposure time of 1200 seconds with the 1m telescope at the CTIO. Basic data reduction techniques were applied using IRAF. Astrometry was performed on the I-band image using the 2MASS catalog by applying IRAF astrometry routines, ‘daofind’, ‘ccxymatch’, and ‘ccmap’. This resulted in a table of sources in the FOV of *Chandra* larger than that of 2MASS due to the I-band observation being deeper than the 2MASS observations.

We performed astrometry on the *Chandra* observations using the data set of I-band sources whose positions were calibrated using the 2MASS catalog. We match the data set of

I band sources to the *Chandra* sources found by WAVDETECT in the full band (0.5-8 keV), in the same manner as discussed above. We find 5 matches with a conservative matching tolerance of $0''.5$, with an RMS of $0''.036$ in the R.A. and $0''.115$ in the Decl. After astrometry was performed on the *Chandra* observations, we find the *Chandra* X-ray detection at the location of 2M1139 is $\sim 0''.25$ from the 2M1139 source in the I-band image. We use the I-band image as the best estimate of position for 2M1139 due to the proximity in time of the *Chandra* observations (2008) and the I-band observation (2007). This was chosen rather than the alternative of using the 2MASS position of 2M1139 and extrapolating the position for the epoch of the *Chandra* observations (2008) from the proper motion found by Scholz et al. (2005b). *Hence, we claim that the detection of 3 photons at the location of 2M1139 is coincident with 2M1139 and thus is a bona fide detection of X-ray emission from 2M1139.*

2M1139 was found to have an absorbed X-ray flux of 5.5×10^{-16} ergs cm $^{-2}$ s $^{-1}$ from the AE output parameter ‘flux2’. Using the distance of $R = 46$ pc determined photometrically by Teixeira et al. (2008), and $L_X = 4\pi R^2 F$ where F is the flux and R is the distance to the target, we determine the X-ray luminosity of 2M1139 to be $L_X = 1.4^{+2.7}_{-1.0} \times 10^{26}$ ergs s $^{-1}$ or $\log L_X/L_{\text{bol}} = -4.8 \pm 0.3$. In determining the error of L_X we have assumed an error in distance of 20% and used the 1σ error in net counts from AE. In determining the error in $\log L_X/L_{\text{bol}}$ we used the 1σ error in net counts from AE only, since $\log L_X/L_{\text{bol}}$ is independent of distance. 2M1139 has a median energy of 1 keV, where TWA 5B has a peak energy of 0.7 keV.

2M1139 was included unsuccessfully in a search for planetary mass companions along with other TW Hydrae objects, HST proposal ID 10176. It is then unlikely that this *Chandra* source may be attributed to a companion or background object to within the resolving power of the NICMOS instrument, the NIC2 has a scale of $0''.075$ pixel $^{-1}$.

Although 2M1139 is near the threshold of detection of *Chandra*, its identification as a detection rather than an upper limit is consistent with the source detection criteria of other publications. Townsley et al. (2006); Broos et al. (2007) use the criteria ‘prob_no_source’ < 0.003 in the full band (0.5-8 keV) as a detection threshold in determining primary sources. Wang et al. (2007, 2010) uses a more conservative criteria of ‘prob_no_source’ < 0.001 in the full band (0.5-8 keV) as a detection threshold in determining primary sources. The ‘prob_no_source’ for 2M1139 in the full band, 6.3×10^{-4} , is well within the above criteria. Townsley et al. (2006) include several sources in their primary source list that like 2M1139 have slightly less than 3 net counts in the full band. A similar detection of a low count source was made by Audard et al. (2007), Kelu-1 an L brown dwarf binary was considered a detection with 4 counts in a 24 ks observation by *Chandra*, a count rate smaller than that of 2M1139. Regardless of the interpretation of the data, the question still remains as to the

discrepancy of the X-ray luminosities between 2M1139 and TWA 5B that are both active as indicated by their H α emission.

3. DISCUSSION

2M1207 and SSSPM 1102 both have strong H α emission, as shown in Figure 1, since they both have H α emission which may be either from a chromosphere or from accretion, we expect they may also have X-ray emission. Stelzer et al. (2006) suggested that accretion may suppress X-ray emission in BDs, where Drake et al. (2009) suggested the opposite, that coronal X-rays modulate the accretion flow in T Tauri stars. Both these mechanisms are consistent with the findings by Preibisch et al. (2005a) for T Tauri stars in the ONC in which they found an anti-correlation between mass accretion rate and X-ray activity.

H α EW is a common criteria in distinguishing accreting, classical T Tauri stars (CTTS), from non-accreting, weak-lined T Tauri stars (WTTS). However, H α EW has no unique cutoff that distinguishes all CTTS from WTTS. This is due to the ‘contrast effect’, different spectral types have different continuums for the same level of chromospheric saturation, causing H α lines to appear more prominent in one spectra type than another (White & Basri 2003). White & Basri (2003) proposed a different diagnostic criterion in distinguishing CTTS (accreting) from WTTS (non-accreting). They propose using the H α 10% FW and a cutoff of 270 km s⁻¹, an H α 10% FW > 270 km s⁻¹ is considered a CTTS (accretor). This criterion, 10% of full width, is independent of the continuum level of stars and thus of the spectral type, and may be a more accurate diagnostic of accretion than H α EW (White & Basri 2003). Jayawardhana et al. (2003) has suggested a modification to the criteria of White & Basri (2003), they adopted an H α 10% FW of \gtrsim 200 km s⁻¹ as a criteria for accretion

Table 1. Brown Dwarfs in TW Hydrae

Name	ST	$v \sin i$ (km s ⁻¹)	H α EW (Å)	H α 10% FW (km s ⁻¹)	L_X (10 ²⁷ ergs s ⁻¹)	$\log(L_X/L_{\text{BOL}})$	References
2M1139	M8	25 \pm 2	9.7, 7.3, 22 \pm 2	111 \pm 10	0.14 ^{+0.27} _{-0.10}	-4.8 \pm 0.3	1, 2, [1,2,3], 2, 4, 4
2M1207	M8	13 \pm 2	27.7, 49 \pm 2, 126	170-320	<0.12	<-4.8	1, 2, [2, 3, 5], 6, 7, 7
TWA 5B	M8.5	16 \pm 2	20, 5.1	162 \pm 10	4	-3.4	8, 2, [9, 2], 2, 8, 8
SSSPM 1102	M8.5	...	10, 64 \pm 3, 50	194	<0.87	<-4.0	10, ..., [10, 3, 5], 11, 6, 4

References. — (1) Gizis (2002); (2) Mohanty et al. (2003); (3) Looper et al. (2007); (4) this work; (5) Herczeg et al. (2009); (6) Stelzer et al. (2007); (7) Gizis & Bharat (2004); (8) Tsuboi et al. (2003); (9) Neuhäuser et al. (2000); (10) Scholz et al. (2005b); (11) Scholz et al. (2005a).

Note. — The multiple measurements of H α EW are listed in chronological order of the cited work. We determined the upper limit on L_X of SSSPM 1102 by converting the upper limit on L_X given by Stelzer et al. (2007) which was based on $d = 43$ pc to an upper limit based on $d = 55.2$ pc determined from trigonometric parallax by Teixeira et al. (2008). We used BC_J from Wilking et al. (1999), m_J from Scholz et al. (2005b), and the distance from Teixeira et al. (2008) in determining L_{bol} for 2M1139 and SSSPM 1102.

Fig. 1.— $H\alpha$ EW measurements for the four BDs of TW Hydrae. The stars represent the X-ray detections of 2M1139 and TWA 5B (Tsuboi et al. 2003), and the arrows represent upper limits. Multiple measurements are listed according to those found in the literature, refer to Table 1.

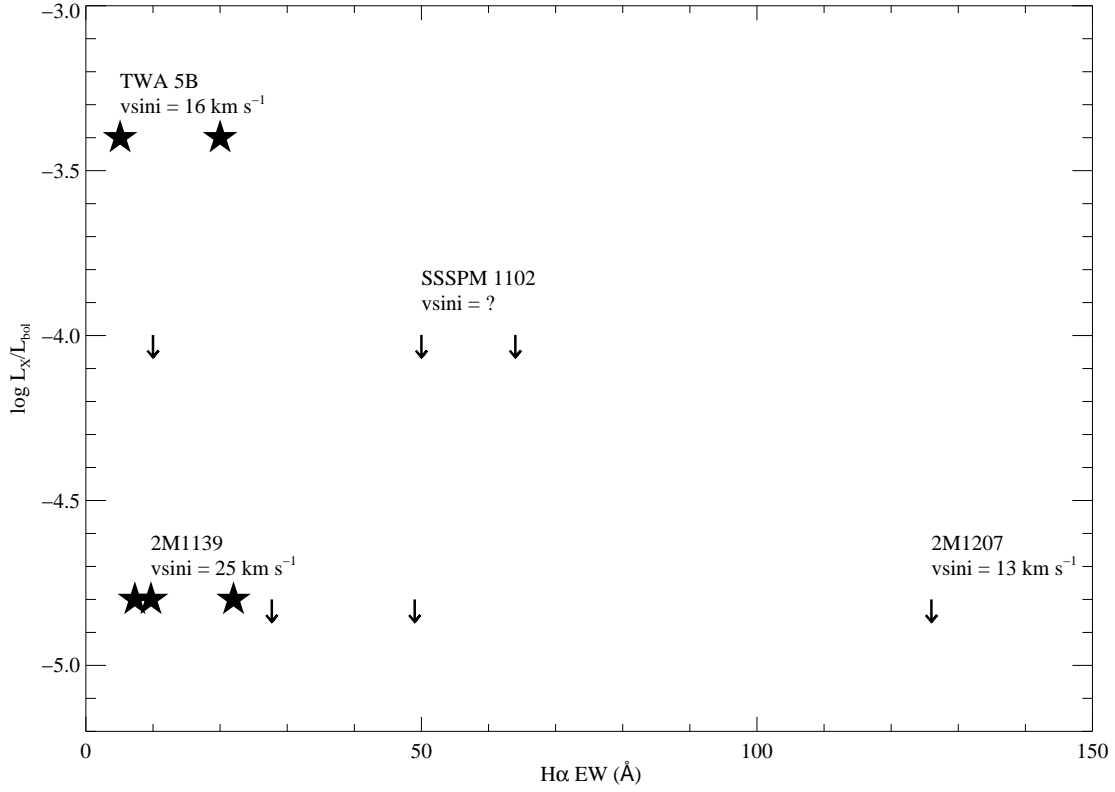
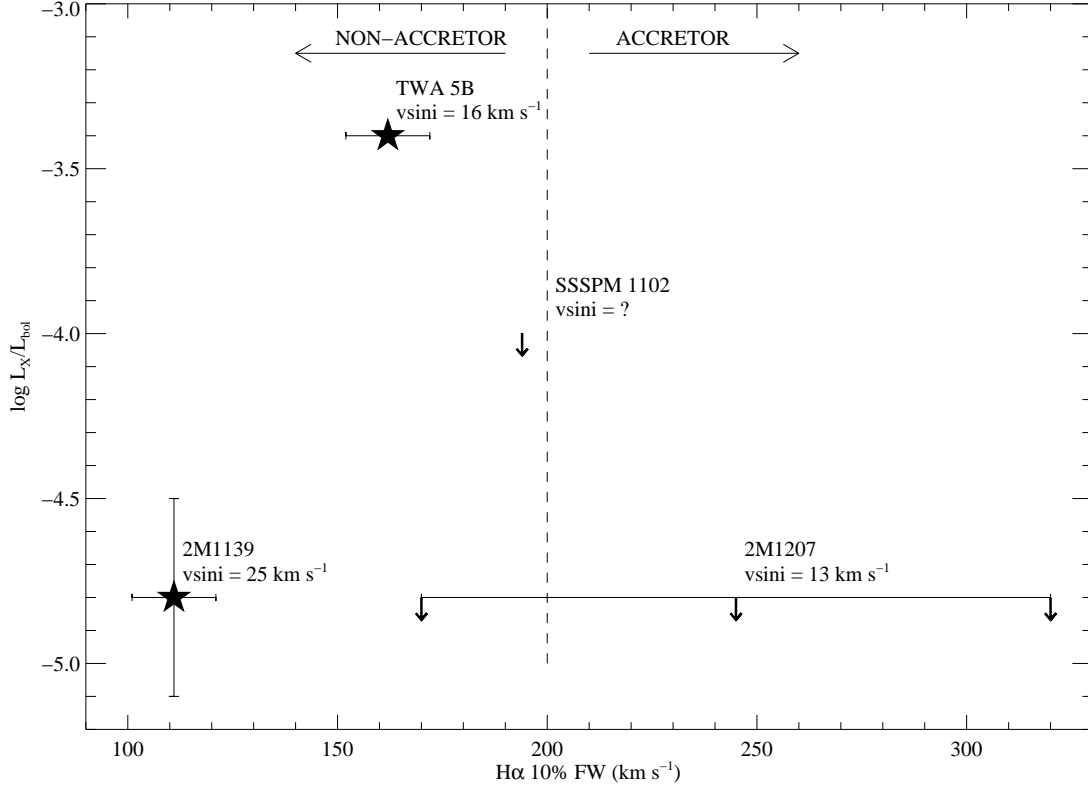


Fig. 2.— $H\alpha$ 10% FW for the four BDs of TW Hydrae. The symbols are the same as in Figure 1. The values of $H\alpha$ 10% FW spanned by 2M1207 show the range due to variability found by Stelzer et al. (2007). The dashed vertical line separates the values of $H\alpha$ 10% FW for an object to be considered an accretor (non-accretor) according to Jayawardhana et al. (2003).



for low mass stars and brown dwarfs. They adopt this criterion over that of White & Basri (2003) because the criteria of $> 270 \text{ km s}^{-1}$ can fail for very low mass objects with low accretion rates (Jayawardhana et al. 2003). We thus adopt the criteria of $\sim 200 \text{ km s}^{-1}$ as a cutoff for accretion, substellar objects with $\gtrsim 200 \text{ km s}^{-1}$ are considered accretors.

2M1207 is considered an accreting substellar object due its large $\text{H}\alpha$ 10% FW emission values (as shown in Figure 2), where SSSPM 1102 is considered an accreting substellar object due its large $\text{H}\alpha$ 10% FW emission value along with measured accretion rates. 2M1207 was found to have variable $\text{H}\alpha$ 10% FW emission by Stelzer et al. (2007), with values ranging from $170\text{--}320 \text{ km s}^{-1}$, where SSSPM 1102 has an $\text{H}\alpha$ 10% FW of 194 km s^{-1} , putting it on the border of accreting. 2M1207 was found to have an accretion rate of $1.3 \times 10^{-12} M_{\odot}/\text{yr}$, and SSSPM 1102 was found to have an accretion rate of $1.6 \times 10^{-13} M_{\odot}/\text{yr}$, both from Balmer emission by Herczeg et al. (2009). 2M1207 was observed by *Chandra* in a 50 ks observation by Gizis & Bharat (2004) with no detection, being given an upper limit of $L_X < 1.2 \times 10^{26} \text{ ergs s}^{-1}$ or $\log L_X/L_{\text{bol}} < -4.8$. Gizis & Bharat (2004) concluded that the $\text{H}\alpha$ emission was from star-disk interactions (accretion). SSSPM 1102 was found in an archival XMM Newton observation by Stelzer et al. (2007), it was not detected and was given an upper limit of $L_X < 8.7 \times 10^{26} \text{ ergs s}^{-1}$ or $\log L_X/L_{\text{bol}} < -4.0$. These X-ray non-detections are consistent with the idea that mass accretion rate and X-ray activity are anti-correlated.

TWA 5B was found to have moderate $\text{H}\alpha$ emission as shown in Figure 1 and Table 1. TWA 5B is not considered an accretor, with an $\text{H}\alpha$ 10% FW of 162 km s^{-1} . TWA 5B was observed and detected in X-rays in a 10.3 ks observation with *Chandra* by Tsuboi et al. (2003). Tsuboi et al. (2003) detected 35 photons, and determined the X-ray emission to be quiescent with an X-ray luminosity of $L_X = 4 \times 10^{27} \text{ ergs s}^{-1}$ or $\log L_X/L_{\text{bol}} = -3.4$.

2M1139 also has moderate $\text{H}\alpha$ emission as shown in Figure 1 and Table 1, values that are quite similar to TWA 5B. It is not an accretor with an $\text{H}\alpha$ 10% FW of 111 km s^{-1} , the lowest of the four BDs in TW Hydrae. We detect X-ray emission from 2M1139 as discussed in section 2.5.

It is not surprising that 2M1139 and TWA 5B have similar $\text{H}\alpha$ EW measurements since chromospheric $\text{H}\alpha$ activity saturates at $v \sin i \approx 10 \text{ km s}^{-1}$ in M5.5–M8.5 dwarfs (Mohanty & Basri 2003), and both 2M1139 and TWA 5B have $v \sin i$ values greater than this. Where the $\text{H}\alpha$ EW measurements of 2M1207 and SSSPM 1102 are greater than and equal to those of 2M1139 and TWA 5B due to accretion and (or) chromospheric activity.

The question is then why does TWA 5B have an X-ray luminosity ~ 10 times greater than 2M1139. Preibisch et al. (2005b) found in the ONC there is an intrinsic range of $\log L_X/L_{\text{bol}}$ for BDs of similar spectral type, with values from $\log L_X/L_{\text{bol}} \approx -3.3$ to -4.2 for

BDs that are of spectral type M6.5-M9, a spread about an order of magnitude. Berger et al. (2010) found from an up to date sample of ultra cool dwarfs, a dispersion of $\log L_X/L_{\text{bol}} \approx -5$ to -3 for M7-M9, where 2M1139 and TWA 5B are well within this range. At this point we may conclude that there is an intrinsic range of X-ray luminosity from BDs of similar spectral types, and 2M1139 and TWA 5B span the lower and upper values of this range. A characteristic that is largely responsible for the range of $\log L_X/L_{\text{bol}}$ for quiescent X-ray emission in main sequence stars with an $\alpha - \Omega$ dynamo is the equatorial rotation velocity, more accurately the Rossby number which is a function of the equatorial rotation velocity (Feigelson et al. 2003). The characteristics responsible for this intrinsic range in fully convective stars is still not understood.

We can rule out flaring as an explanation for the large X-ray emission of TWA 5B compared to 2M1139. Flaring is unlikely considering that Tsuboi et al. (2003) found it to be quiescent over a 10 ks observation. TWA 5B does not show the rise and decay of a flare. Berger et al. (2010) found ultracool dwarfs to have typical flaring durations of approximately 1 hour, with a range of about 10^2 to 10^4 seconds, thus the rise or decay of a flare from TWA 5B would probably have been seen during the 10 ks observation.

We compare and contrast 2M1139 and TWA 5B: both have $H\alpha$ emission, both show no signatures of accretion, and have comparable ages and spectral types. In an effort to exploit discrepancies between the two to understand why one has high X-ray emission near the saturation limit and the other has very low X-ray emission, we examine the equatorial rotation velocity and X-ray emission of 2M1139 and TWA 5B.

3.1. Rotation

Mohanty & Basri (2003) looked at fully convective objects, M4-L6, analyzing the activity-rotation relation for chromospheric activity ($H\alpha$ emission). They found that for M4-M8.5 a saturation type activity-rotation relation exists for chromospheric activity ($H\alpha$ emission), extending the work on $H\alpha$ activity from Delfosse et al. (1998) into the late M spectral type. They also find a drastic drop in $H\alpha$ activity for spectral type $\geq M9$. This may be the result of very high resistivities in the neutral atmospheres, perhaps combined with the rapid formation of dust, which would damp magnetic energy available for supporting a chromosphere (Mohanty & Basri 2003). Mohanty & Basri (2003) use $v \sin i$ as a measure of rotation, and is limited because it only gives a lower limit on the equatorial rotation velocity. Nonetheless, from these works it is clear there is a saturation plateau for fully convective objects.

Work by Berger et al. (2008a), Berger et al. (2008b), and Berger et al. (2010) are

beginning to piece together the picture of activity in fully convective objects of spectral type $>M7$. Their work finds a distinct change in activity around spectral type $\sim M7$. They find a decline in X-ray activity for spectral type $\geq M7$, and a decline in $H\alpha$ activity at $\geq M6$, slightly earlier in spectral type than Mohanty & Basri (2003).

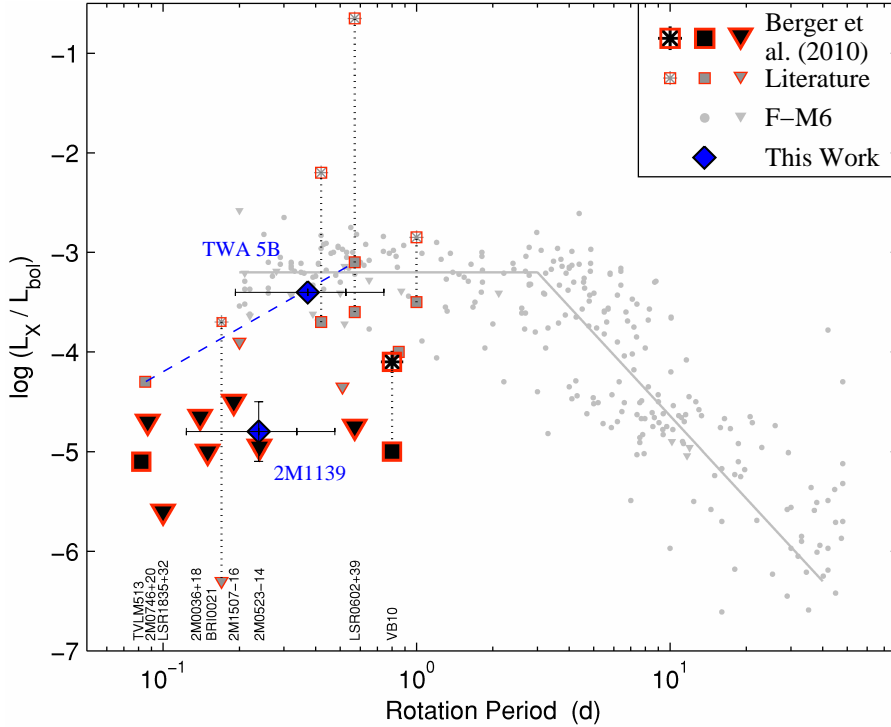
Berger et al. (2010), Figure 9, examine the activity-rotation relation of ultracool dwarfs and find for moderate rotators, $1 > P > 0.3$ days, a median $\log L_X/L_{\text{bol}} = -4$. Fast rotators, $P < 0.3$ days, are found to generally have weaker X-ray emission, a median $\log L_X/L_{\text{bol}} = -5$, and they suggest that this may be analogous to the super saturation regime for main sequence objects. Ultracool dwarfs that are moderate rotators saturate at $\log L_X/L_{\text{bol}} = -3$, like main sequence stars. But unlike the main sequence activity-rotation relation for X-ray emission, based on detections there exists a large dispersion below the saturation plateau, from $\log L_X/L_{\text{bol}} \approx -5$ to -3 . All of the detections are from spectral types M7-M9, with the exception of the L2, Kelu-1, with $\log L_X/L_{\text{bol}} = -4.3$. Berger et al. (2010) notes that this is based on a small number of objects and needs to be confirmed with larger numbers, but it suggests the possibility of a super saturation regime. A number of possible explanations for the super saturation region have been proposed, intrinsic dynamo effects, secondary effects of centrifugal stripping, or that the source of coronal heating is different (inefficient heating) (Berger et al. 2008b).

Periods of 2M1139 and TWA 5B are not known, but we can determine a spread of values for period given their $v \sin i$ values and a few select inclinations. We use $P = (2\pi R)/v$ where $v = V/\sin i$, P is the period, R is the radius, v is the equatorial rotation velocity, i is the inclination, and V is the measured $v \sin i$ value. We used the radius of 2M1207 as an estimate for the radii of 2M1139 and TWA 5B in determining the period due to similarities in age and mass. We inferred the radius of 2M1207 directly from the L_{bol} and T_{eff} from Mohanty et al. (2007).

Figure 3 shows the activity-rotation relation for X-ray activity in ultracool dwarfs, taken from Figure 9 of Berger et al. (2010), with the results of this work overlaid as diamond symbols. The four tick marks for 2M1139 and TWA 5B show, from left to right, inclinations of 15° , 30° , 45° , and 90° . The dashed line shows the approximate upper envelope for quiescent X-ray detections for this figure, where the lower envelope is not well defined based on only 2 detections and many upper limits. X-ray activity is shown to have considerable scatter, $-5 < \log L_X/L_{\text{bol}} < -3$ for moderate rotators, $P > 0.3$ days, and for the scatter to decrease as the period decreases. *The detections of 2M1139 and TWA 5B span this scatter in X-ray activity. Though rotation may play a role in the X-ray activity of ultracool dwarfs, the discrepancy between 2M1139 and TWA 5B cannot be explained by rotation alone.*

Rice et al. (2010) gives different $v \sin i$ values for 2M1139 and TWA 5B than those

Fig. 3.— Figure 9 from Berger et al. (2010), with the data from 2M1139 and TWA 5B of this work overlaid as diamond symbols. The four tick marks for 2M1139 and TWA 5B represent, from left to right, an inclination of 15° , 30° , 45° , and 90° . The dashed line represents the approximate upper envelope of quiescent X-ray detections for this plot, based on a small sample size of $\geq M7$ dwarfs. The lower envelope is not well defined based on only 2 detections and many upper limits. This figure shows that rotation may play a role in the X-ray activity of ultracool dwarfs like 2M1139 and TWA 5B, but due to the dispersion of $\log L_X/L_{\text{bol}}$ below the upper envelope, rotation alone cannot explain the difference in X-ray emission between 2M1139 and TWA 5B.



determined by Mohanty et al. (2003), Table 1. They report a $v \sin i$ of 30 km s^{-1} for 2M1139 and 27 km s^{-1} for TWA 5B. The value of $v \sin i$ for TWA 5B is an increase of about 70% over that of Mohanty et al. (2003). Their measurements for the $v \sin i$ values of field objects have disparities with previous measurements as well, twice the previous measured value for 2MASS 0140+27 and three times the previous measured value for LP 412-31. Rice et al. (2010) note that their temperatures measured from spectral fitting for TWA 5B and these field objects are hotter than previously determined temperatures. They argue this is likely a consequence of increasing importance on FeH absorption for cooler and higher gravity objects that isn't reproduced by the atmosphere models they used. Also, that their spectra for TWA 5B has a low signal to noise and that it may be contaminated by its bright primary. Considering that Mohanty et al. (2003) gives errors of $\pm 2 \text{ km s}^{-1}$ for their $v \sin i$ measurements, and the issues discussed above for TWA 5B, we thus consider the measurements of $v \sin i$ by Mohanty et al. (2003) to be more reliable and use these in our analysis.

Vacca & Sandell (2011) find an age for TW Hya, and thus of the coevolved TW Hydrae association, of $\sim 3 \text{ Myr}$. This age is in contrast to the older accepted age of $\sim 8 - 10 \text{ Myr}$. There are a number of characteristics that may be expected to change with age if these BDs in TW Hydrae are actually $\sim 3 \text{ Myr}$ rather than the accepted age of $\sim 8 - 10 \text{ Myr}$. In discussing these characteristics based on age we must exclude TW Hydrae BDs from the analysis of cited work since its age is the topic of discussion. According to Zapatero Osorio et al. (2006) the projected rotational velocity would be slightly lower because BDs spin up with age due to gravitational contraction. From Stelzer et al. (2006) the effective temperature would be slightly higher. Without the detection of TWA 5B at $\sim 10 \text{ Myr}$, a relation between X-ray plasma temperature and age becomes ambiguous (Tsuboi et al. 2003). There appears to be no clear relation between age and $\log L_X/L_{\text{bol}}$ (Stelzer 2004; Tsuboi et al. 2003), except to say that we still see moderate X-ray activity at ages of several hundred million years, Gl 569Bab (Stelzer 2004). No assumptions about the age of TW Hydrae have been made in our analysis of 2M1139 and the BDs of TW Hydrae. Furthermore, our analysis comparing and contrasting the BDs of TW Hydrae is age independent since they are coevolved. Thus, a younger age of $\sim 3 \text{ Myr}$ by Vacca & Sandell (2011) for TW Hydrae has no effect on our conclusions.

4. CONCLUSIONS

We report a 3σ detection of 2M1139 in X-rays with $L_X = 1.4^{+2.7}_{-1.0} \times 10^{26} \text{ ergs s}^{-1}$ or $\log L_X/L_{\text{bol}} = -4.8 \pm 0.3$. 2M1139 is similar in $H\alpha$ activity, lack of accretion signatures, age, and spectral type to TWA 5B, another BD in TW Hydrae, yet TWA 5B has ~ 10 times the

X-ray luminosity. We find the span in $\log L_X/L_{\text{bol}}$ between these two objects is consistent with BDs of similar spectral types in the ONC (Preibisch et al. 2005b). Based on recent work on the activity-rotation relation for X-ray activity of fully convective objects (Berger et al. 2010), we find that rotation may play a role in the X-ray activity of ultracool dwarfs like 2M1139 and TWA 5B. However, due to the large span in $\log L_X/L_{\text{bol}}$ of detections, which is comparable to the span of $\log L_X/L_{\text{bol}}$ between 2M1139 and TWA 5B, the discrepancy cannot be explained by rotation alone.

Future work should include X-ray observations of DENIS 1245. If found to be a bona fide member of TW Hydrae, further study would help to complete the picture of substellar objects at an age of ~ 10 Myr. DENIS 1245 has detected H α emission with an H α EW of 15 Å (Looper et al. 2007), so we know it to be active. If DENIS 1245 is found to have X-ray emission, its place in context to the other four BDs of TW Hydrae, specifically 2M1139 and TWA 5B, will help to shape our understanding of X-ray activity of BDs at the age of ~ 10 Myr.

5. ACKNOWLEDGMENTS

Support for this work was provided by NASA research grant NNG06GJ03G. Support for this work was provided by the National Aeronautics and Space Administration through *Chandra* Award Number GO89011X issued by the *Chandra* X-ray Observatory Center, which is operated by the Smithsonian Astrophysical Observatory for and on behalf of the National Aeronautics Space Administration under contract NAS8-03060. This work has made use of telescopes operated by the SMARTS consortium. This publication makes use of data products from the Two Micron All Sky Survey, which is a joint project of the University of Massachusetts and the Infrared Processing and Analysis Center/California Institute of Technology, funded by the National Aeronautics and Space Administration and the National Science Foundation. This research has made use of the SIMBAD database, operated at CDS, Strasbourg, France. This research also makes use of the ACIS Extract software package maintained at Pennsylvania State University. We thank Dr. James MacDonald for many useful discussions. We thank the anonymous referee for suggestions that helped to improve the manuscript.

A. CHANDRA X-RAY SOURCES IN THE FOV

A.1. Table 2

Table 2. *Chandra* X-Ray Sources in the FOV

IAU Designation (J2000) (1)	R.A. (J2000) (2)	Decl. (J2000) (3)	Full Band: 0.5 – 8 keV			Soft Band: 0.5 – 2 keV		
			Net Counts (4)	Absorbed Flux 10^{-16} (ergs cm $^{-2}$ s $^{-1}$) (5)	Median Energy (keV) (6)	Net Counts (7)	Absorbed Flux 10^{-16} (ergs cm $^{-2}$ s $^{-1}$) (8)	
J113924.6-315923	174.85276	-31.989982	75.97 $^{+9.88}_{-8.81}$	340.6	1.1	63.25 $^{+7.98}_{-7.98}$	168.6	
J113926.0-315941	174.85865	-31.994910	24.05 $^{+6.17}_{-5.06}$	107.1	1.4	14.38 $^{+4.97}_{-3.86}$	38.2	
J113926.6-320107	174.86101	-32.018644	196.08$^{+10.10}_{-14.06}$	869.0	1.0	187.27$^{+13.74}_{-13.70}$	495.0	
J113931.7-315841	174.88215	-31.978158	6.18 $^{+3.78}_{-2.58}$	26.6	3.5	0.71 $^{+0.83}_{-0.83}$	1.8	
J113931.9-315540	174.88311	-31.927813	15.68 $^{+5.21}_{-4.21}$	69.5	1.6	10.63 $^{+4.43}_{-3.26}$	29.9	
J113942.9-315553	174.92897	-31.931590	57.85 $^{+8.73}_{-7.66}$	116.7	1.0	51.63 $^{+8.26}_{-7.19}$	65.8	
J113944.9-320249	174.93740	-32.047128	10.47 $^{+4.43}_{-2.94}$	44.8	1.8	6.81 $^{+3.78}_{-2.32}$	18.1	
J113947.2-320010	174.94701	-32.002880	2.84 $^{+2.94}_{-1.63}$	5.6	3.7	0.95 $^{+2.32}_{-0.83}$	1.1	
J113947.3-315613	174.94744	-31.936991	74.39 $^{+9.70}_{-8.64}$	148.1	1.4	51.74 $^{+8.26}_{-7.19}$	63.4	
J113947.6-320024	174.94841	-32.006832	12.82 $^{+3.55}_{-3.14}$	25.2	1.8	6.96 $^{+2.58}_{-2.19}$	8.2	
J113950.6-320038	174.96110	-32.010591	16.81 $^{+5.21}_{-4.08}$	32.9	1.2	9.95 $^{+4.28}_{-3.10}$	11.7	
J113951.0-315921	174.96284	-31.989374	2.84$^{+2.94}_{-3.40}$	5.5	1.0	2.95$^{+2.94}_{-2.32}$	3.4	
J113951.6-315723	174.96539	-31.956664	4.74 $^{+2.15}_{-3.96}$	9.3	3.8	0.92 $^{+0.83}_{-0.60}$	1.1	
J113952.7-315709	174.96974	-31.952770	7.70 $^{+3.96}_{-5.09}$	15.3	1.4	5.89 $^{+3.60}_{-2.71}$	7.0	
J113953.9-315830	174.97481	-31.975213	15.85 $^{+5.09}_{-3.95}$	31.0	1.1	12.96 $^{+4.71}_{-3.55}$	15.2	
J113954.1-315807	174.97574	-31.968710	40.81 $^{+7.46}_{-6.37}$	79.6	1.4	30.94 $^{+6.63}_{-5.53}$	36.3	
J113956.2-320005	174.98438	-32.001403	6.85 $^{+2.58}_{-2.12}$	13.4	1.8	3.94 $^{+3.18}_{-3.60}$	4.6	
J113956.7-315852	174.98626	-31.981228	8.82 $^{+2.94}_{-5.33}$	17.3	1.4	5.94 $^{+2.37}_{-3.60}$	7.0	
J113956.8-315623	174.98699	-31.939751	17.43 $^{+5.33}_{-4.57}$	35.5	0.9	15.84 $^{+5.09}_{-3.60}$	19.4	
J113958.3-320305	174.99300	-32.051401	11.19 $^{+3.41}_{-4.57}$	23.4	1.9	5.71 $^{+3.60}_{-2.37}$	7.6	
J114001.2-315503	175.00511	-31.917502	28.47 $^{+6.55}_{-5.96}$	111.5	1.6	22.68 $^{+5.87}_{-4.71}$	53.3	
J114004.6-320040	175.01927	-32.011213	780.56$^{+28.96}_{-27.94}$	2950.3	1.0	734.76$^{+28.12}_{-27.10}$	1700.0	
J114014.8-315527	175.06200	-31.924189	4.39 $^{+3.98}_{-2.79}$	18.4	4.3	1.03 $^{+2.67}_{-1.30}$	2.5	
J114015.7-315844	175.06565	-31.978890	8.23 $^{+3.48}_{-3.41}$	32.0	2.0	3.57 $^{+1.93}_{-1.93}$	8.5	
J114018.3-315654	175.07654	-31.948447	30.61 $^{+6.90}_{-5.81}$	125.0	2.4	10.86 $^{+4.58}_{-3.42}$	26.3	

Note. — The rows in bold highlight 2M1139 and the two objects of interest in the FOV of the *Chandra* observations.

For completeness we have provided the output from ACIS Extract for the entire FOV of our *Chandra* observations. Table 2 shows the sources detected by WAVDETECT with scales 1, 2, 4, 8, and 16, with a significance threshold of 5×10^{-7} , and 2M1139 which was detected in the soft band image, 0.1-1.5 keV, under the same scales and significance threshold. Column 1 is the IAU designation in J2000 for each source, and columns 2 and 3 are the Right Ascension and Declination in J2000, respectively. Columns 4 to 6 show the full band (0.5-8 keV), and 7 and 8 show the soft band (0.5-2 keV) output. Columns 4 and 7 are the net counts, and columns 5 and 8 are the absorbed flux from the output parameter ‘flux2’. Column 6 is the median energy, ‘energ_pct50_observed’, which is the background subtracted median observed energy, where the observed energy is based on net counts rather than the ‘energ_pct50_incident’ which is based on flux.

A.2. J114004.6-320040

An X-ray source in the FOV of our *Chandra* observations that warranted further investigation was J114004.6-320040, 2MASS source J11400464-3200411. This was the brightest X-ray source in the FOV, having almost 800 counts. It was detected by GALEX in the near-ultraviolet (NUV) and far-ultraviolet (FUV).

The light-curve for J114004.6-320040 is shown in Figure 4 (top). The KS statistic yields a probability of 0.01, or that there is a 99% probability that the object is variable. We applied the maximum likelihood method to the light-curve of J114004.6-320040 and found that within 95% confidence that it was variable between the first (1.9 hrs) 7 ks and the last (2.6 hrs) 9 ks, due to the count rate jump at (1.9 hrs) 7 ks.

We use the CIAO routine PSEXTRACT and the spectral fitting package XSPEC to fit the spectra of J114004.6-320040 (Figure 5, top left) with a two temperature APEC (Wilm abund) model. We find a good fit with $kT_1 = 0.73 \pm 0.04$ keV, $kT_2 = 2.2 \pm 0.4$ keV, and a column density of $N_H = 1.0 \pm 0.3 \times 10^{21} \text{ cm}^{-2}$. We find an unabsorbed flux of $f_{xu} = 1.5 \times 10^{-13} \text{ ergs cm}^{-2} \text{ s}^{-1}$ and an absorbed flux of $f_{xa} = 1.3 \pm 0.1 \times 10^{-13} \text{ ergs cm}^{-2} \text{ s}^{-1}$.

This object was observed at the CTIO by the 1.5m spectrograph using grating 32/I, over a wavelength of ~ 6000 to 9000 \AA , with a resolution of $\sim 3 \text{ \AA pixel}^{-1}$. Four observations were obtained on March 10, 2010, with an exposure time of 100 seconds each. The data was reduced with standard IRAF procedures and were combined to obtain the best signal to noise.

We used the spectral standards of Danks & Dennefeld (1994) which covered our entire wavelength range and was similar to our resolution at 4 \AA pixel^{-1} . We used absorption

Fig. 4.— Light curves for the two objects of interest in the FOV of the *Chandra* observations. Light-curves are binned over 1 ks. Top: Light-curve for object J114004.6-320040 that was observed during ObsId 9841 only. Bottom: Light-curve for object J113926.6-320107 from ObsId 9835 (bottom left) which shows quiescent emission and ObsId 8913 (bottom right) which clearly shows the decay phase of a flare.

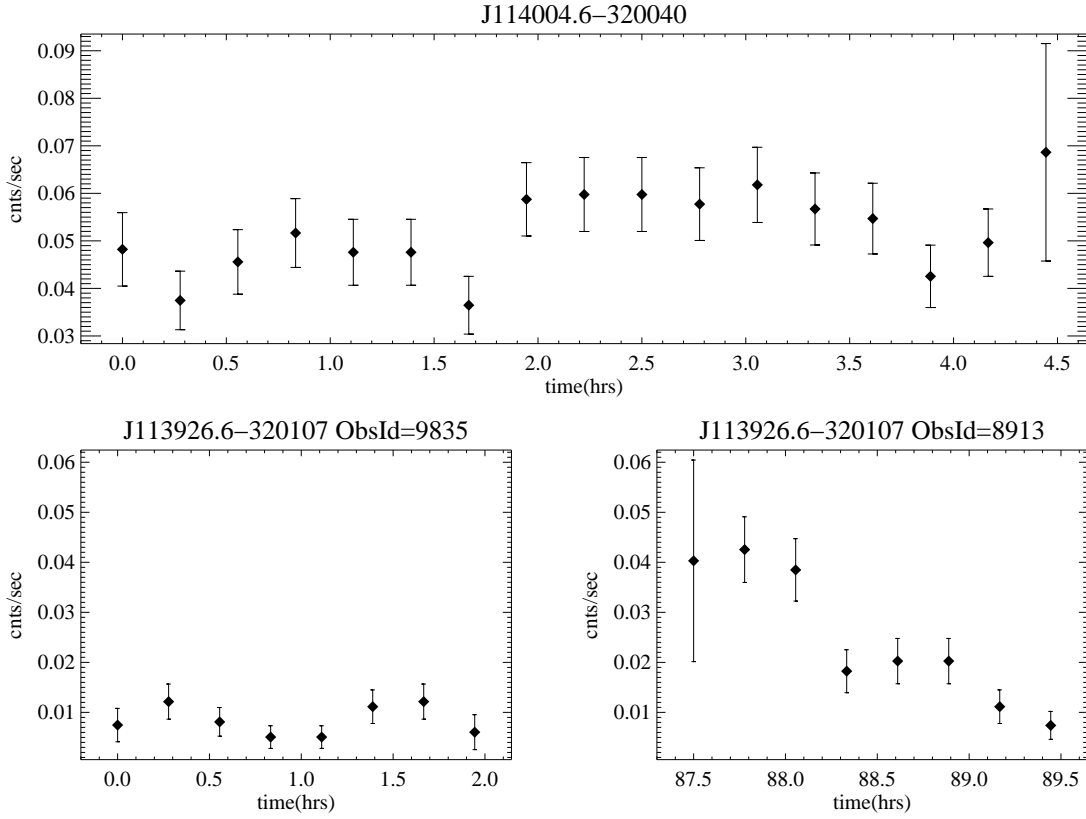
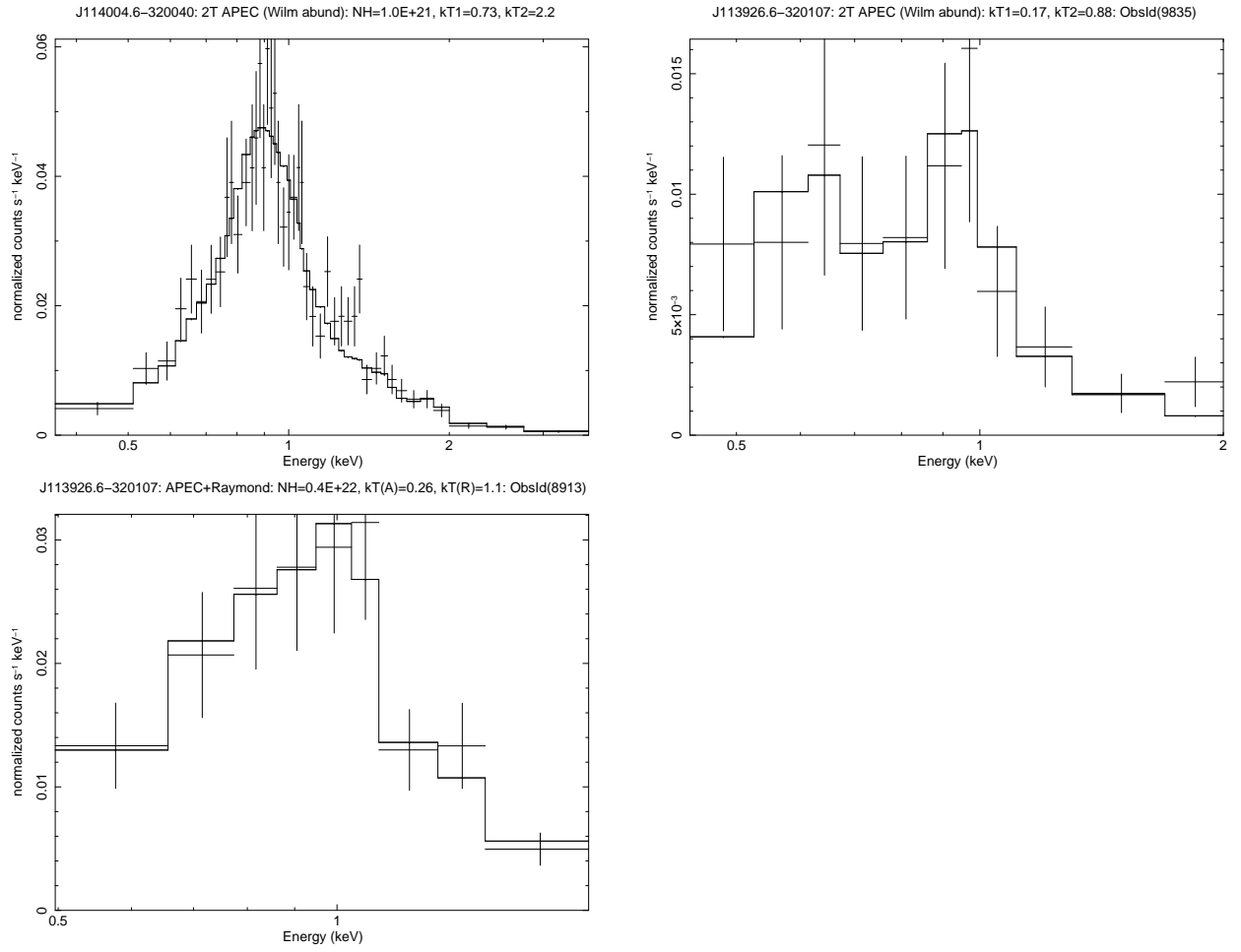


Fig. 5.— *Chandra* spectra of J114004.6-320040 and J113926.6-320107 for ObsId 9835 (quiescent) and ObsId 8913 (flaring).



features of Ca I at 6162 Å, the blended line of Ba II, Fe I, and Ca I at 6497 Å, and the Mg I line at 8807 Å to determine the spectral type of J114004.6-320040 (Danks & Dennefeld 1994; Allen & Strom 1995; Torres-Dodgen & Weaver 1993). The H α line at 6563 Å, and the Ca II triplet at 8498, 8542, and 8662 Å, all show filling, which is indicative of chromospheric activity, refer to Figure 6. The Ca II triplet is formed in the lower chromosphere and shares the upper level of the Ca II H & K transitions, which are the most widely used optical indicators of chromospheric activity. The H α line is formed at the middle chromosphere and in less active stars only has a filled in absorption line (Montes et al. 2004; Mallik 1994, 1997).

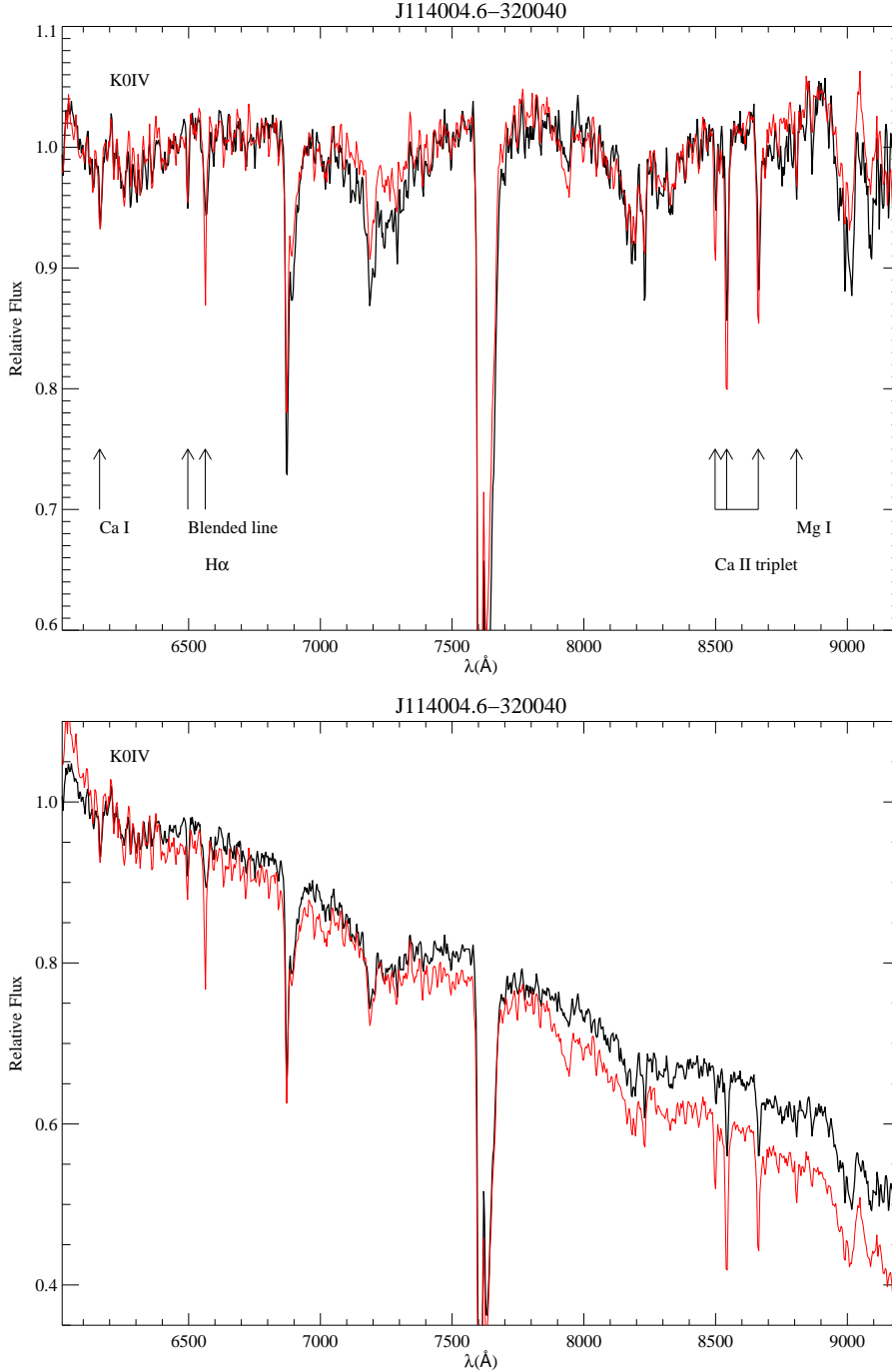
Based on the absorption spectral features mentioned above in conjunction with the slope of the flux calibrated spectra continuum to that of the standard, we find this object to be of spectral type K0IV. The flux calibrated spectra is consistent with the standard but shows interstellar reddening (refer to Figure 6). With this spectral classification, we have $\log L_X/L_{\text{bol}} = -3.6$, using $BC_V = -0.4$ which is the average of the BC_V for the main sequence K0V, which gives $\log L_X/L_{\text{bol}} = -3.5$, and the giant K0III, which gives $\log L_X/L_{\text{bol}} = -3.6$ (Cox, A. N. 2000).

Single subgiants are generally not known to be strong X-ray emitters, and overall show low activity (Dorren et al. 1995; Walter et al. 1980). One of the nearest subgiants, β Hyi, was found by ROSAT to have an X-ray luminosity of $L_X = (0.9 - 3.0) \times 10^{27} \text{ ergs s}^{-1}$ (Dorren et al. 1995). As stars evolve their rotation rates decrease through magnetic braking which is accompanied by a parallel decrease in the various measures of stellar activity (Dempsey et al. 1993). However, RS Canum Venaticorum (RS CVn) binary systems are of the most luminous stellar coronal X-ray sources, having X-ray flux orders of magnitude more than slowly rotating single late-type stars, $L_X \sim 10^{29-31.5} \text{ ergs s}^{-1}$ (Osten et al. 2000; Dempsey et al. 1993). RS CVns usually consist of a G or K-type giant or subgiant with a late-type main sequence or subgiant companion, where the definition of these systems was first defined by Hall (1976) (Dempsey et al. 1993). These are systems that have fast rotation because tidal forces have caused the rotation period to be synchronized with the orbital period, ≤ 30 days, where this rapid rotation enhances stellar activity (Osten et al. 2000; Dempsey et al. 1993). We classify J114004.6-320040 as a RS CVn, K0IV. We saw no evidence of binarity based on our low-dispersion spectra. Follow-up, higher-dispersion (preferably echelle) spectral monitoring is needed to confirm this object as a bona fide RS CVn.

A.3. J113926.6-320107

We analyze the second brightest object in the FOV of our *Chandra* observations, with almost 200 counts. This object was found in the 2MASS catalog and was detected by GALEX

Fig. 6.— Spectra of J114004.6-320040 (thick black line) with comparison standard spectra (thin red line) of Danks & Dennefeld (1994). Top: Normalized spectra showing the best fit standard spectra of K0IV. Absorption features that were used to classify the spectral type and those that show filling are labeled. Bottom: Flux calibrated spectra showing interstellar reddening of J114004.6-320040 compared to the standard.



in the NUV and the FUV. No object was found in the SIMBAD database within $2''$ of the R.A. and Decl.

The light-curve for J113926.6-320107 is shown in Figure 4 (bottom) with clear variability. ObsId 9835 has a KS probability of 0.4, the object is considered quiescent during this observation. ObsId 8913 has a KS probability of 8×10^{-7} , the light-curve with great confidence is variable. Qualitatively, ObsId 8913 clearly shows the decay phase of a flare whose rise has occurred at some time between ObsId 9835 and ObsId 8913.

We analyze the spectra of J113926.6-320107 separately for ObsId 9835 and ObsId 8913 since the former is of quiescent emission and the latter is during the decay phase of a flare. We fit the spectra of ObsId 9835 (Figure 5, top right) with a two temperature APEC (Wilm abund) model. We find a good fit with $kT_1 = 0.17 \pm 0.05$ keV, $kT_2 = 0.88 \pm 0.23$ keV, and a fixed column density from ObsId 8913 of $N_H = 0.4 \pm 0.4 \times 10^{22} \text{ cm}^{-2}$. We find an unabsorbed flux of $f_{xu} = 1.3 \times 10^{-13} \text{ ergs cm}^{-2} \text{ s}^{-1}$ and an absorbed flux of $f_{xa} = 3.3^{+0.3}_{-1.8} \times 10^{-14} \text{ ergs cm}^{-2} \text{ s}^{-1}$. We fit the spectra of ObsId 8913 (Figure 5, bottom) with a two temperature APEC+Raymond (Wilm abund) model. We find a good fit with $kT_{\text{APEC}} = 0.26 \pm 0.10$ keV, $kT_{\text{Raymond}} = 1.1 \pm 0.1$ keV, and a column density of $N_H = 0.4 \pm 0.4 \times 10^{22} \text{ cm}^{-2}$. We find an unabsorbed flux of $f_{xu} = 2.4 \times 10^{-13} \text{ ergs cm}^{-2} \text{ s}^{-1}$ and an absorbed flux of $f_{xa} = 9.7^{+0.3}_{-4.9} \times 10^{-14} \text{ ergs cm}^{-2} \text{ s}^{-1}$.

REFERENCES

- Allen, L. E., & Strom, K. M. 1995, *AJ*, 109, 1379
- Audard, M., Osten, R. A., Brown, A., Briggs, K. R., Güdel, M., Hodges-Kluck, E., & Gizis, J. E. 2007, *A&A*, 471, L63
- Berger, E., et al. 2008a, *ApJ*, 673, 1080
- . 2008b, *ApJ*, 676, 1307
- . 2010, *ApJ*, 709, 332
- Briggs, K. R., & Pye, J. P. 2004, *MNRAS*, 353, 673
- Broos, P. S., Feigelson, E. D., Townsley, L. K., Getman, K. V., Wang, J., Garmire, G. P., Jiang, Z., & Tsuboi, Y. 2007, *ApJS*, 169, 353
- Broos, P. S., Townsley, L. K., Feigelson, E. D., Getman, K. V., Bauer, F. E., & Garmire, G. P. 2010, *ApJ*, 714, 1582

- Browning, M. K. 2008, *ApJ*, 676, 1262
- Chabrier, G., & Baraffe, I. 1997, *A&A*, 327, 1039
- Chabrier, G., & Küker, M. 2006, *A&A*, 446, 1027
- Charbonneau, P. 2010, *Living Reviews in Solar Physics*, 7, 3
- Cox, A. N., ed. 2000, *Allen’s Astrophysical Quantities* (New York: Springer)
- Cram, L. E. 1982, *ApJ*, 253, 768
- Danks, A. C., & Dennefeld, M. 1994, *PASP*, 106, 382
- Delfosse, X., Forveille, T., Perrier, C., & Mayor, M. 1998, *A&A*, 331, 581
- Dempsey, R. C., Linsky, J. L., Fleming, T. A., & Schmitt, J. H. M. M. 1993, *ApJS*, 86, 599
- Dorren, J. D., Guedel, M., & Guinan, E. F. 1995, *ApJ*, 448, 431
- Drake, J. J., Ercolano, B., Flaccomio, E., & Micela, G. 2009, *ApJ*, 699, L35
- Durney, B. R., De Young, D. S., & Roxburgh, I. W. 1993, *Sol. Phys.*, 145, 207
- Feigelson, E. D., Broos, P., Gaffney, III, J. A., Garmire, G., Hillenbrand, L. A., Pravdo, S. H., Townsley, L., & Tsuboi, Y. 2002, *ApJ*, 574, 258
- Feigelson, E. D., Gaffney, III, J. A., Garmire, G., Hillenbrand, L. A., & Townsley, L. 2003, *ApJ*, 584, 911
- Fleming, T. A., Liebert, J., Gioia, I. M., & Maccacaro, T. 1988, *ApJ*, 331, 958
- Gagné, M., Skinner, S. L., & Daniel, K. J. 2004, *ApJ*, 613, 393
- Gizis, J. E. 2002, *ApJ*, 575, 484
- Gizis, J. E., & Bharat, R. 2004, *ApJ*, 608, L113
- Gizis, J. E., Monet, D. G., Reid, I. N., Kirkpatrick, J. D., Liebert, J., & Williams, R. J. 2000, *AJ*, 120, 1085
- Grosso, N., et al. 2007, *A&A*, 468, 391
- Hall, D. S. 1976, in *Astrophysics and Space Science Library*, Vol. 60, IAU Colloq. 29: Multiple Periodic Variable Stars, ed. W. S. Fitch, 287–+

- Herczeg, G. J., Cruz, K. L., & Hillenbrand, L. A. 2009, *ApJ*, 696, 1589
- Imanishi, K., Tsujimoto, M., & Koyama, K. 2001, *ApJ*, 563, 361
- Jayawardhana, R., Mohanty, S., & Basri, G. 2003, *ApJ*, 592, 282
- Looper, D. L., Burgasser, A. J., Kirkpatrick, J. D., & Swift, B. J. 2007, *ApJ*, 669, L97
- Lowrance, P. J., et al. 1999, *ApJ*, 512, L69
- Mallik, S. V. 1994, *A&AS*, 103, 279
- . 1997, *A&AS*, 124, 359
- Mamajek, E. E. 2005, *ApJ*, 634, 1385
- Mohanty, S., & Basri, G. 2003, *ApJ*, 583, 451
- Mohanty, S., Jayawardhana, R., & Barrado y Navascués, D. 2003, *ApJ*, 593, L109
- Mohanty, S., Jayawardhana, R., Huélamo, N., & Mamajek, E. 2007, *ApJ*, 657, 1064
- Montes, D., Crespo-Chacón, I., Gálvez, M. C., Fernández-Figueroa, M. J., López-Santiago, J., de Castro, E., Cornide, M., & Hernán-Obispo, M. 2004, *Lecture Notes and Essays in Astrophysics*, 1, 119
- Neuhauser, R., & Comeron, F. 1998, *Science*, 282, 83
- Neuhäuser, R., Guenther, E. W., Petr, M. G., Brandner, W., Huélamo, N., & Alves, J. 2000, *A&A*, 360, L39
- Neuhäuser, R., et al. 1999, *A&A*, 343, 883
- Osten, R. A., Brown, A., Ayres, T. R., Linsky, J. L., Drake, S. A., Gagné, M., & Stern, R. A. 2000, *ApJ*, 544, 953
- Parker, E. N. 1955, *ApJ*, 122, 293
- Preibisch, T., & Zinnecker, H. 2002, *AJ*, 123, 1613
- Preibisch, T., et al. 2005a, *ApJS*, 160, 401
- . 2005b, *ApJS*, 160, 582
- Rice, E. L., Barman, T., Mclean, I. S., Prato, L., & Kirkpatrick, J. D. 2010, *ApJS*, 186, 63

- Rutledge, R. E., Basri, G., Martín, E. L., & Bildsten, L. 2000, *ApJ*, 538, L141
- Scholz, A., Jayawardhana, R., & Brandeker, A. 2005a, *ApJ*, 629, L41
- Scholz, R., McCaughrean, M. J., Zinnecker, H., & Lodieu, N. 2005b, *A&A*, 430, L49
- Song, I., Zuckerman, B., & Bessell, M. S. 2003, *ApJ*, 599, 342
- Stelzer, B. 2004, *ApJ*, 615, L153
- Stelzer, B., Micela, G., Flaccomio, E., Neuhäuser, R., & Jayawardhana, R. 2006, *A&A*, 448, 293
- Stelzer, B., Scholz, A., & Jayawardhana, R. 2007, *ApJ*, 671, 842
- Teixeira, R., Ducourant, C., Chauvin, G., Krone-Martins, A., Song, I., & Zuckerman, B. 2008, *A&A*, 489, 825
- Torres-Dodgen, A. V., & Weaver, W. B. 1993, *PASP*, 105, 693
- Townsley, L. K., Broos, P. S., Feigelson, E. D., Garmire, G. P., & Getman, K. V. 2006, *AJ*, 131, 2164
- Tsuboi, Y., Maeda, Y., Feigelson, E. D., Garmire, G. P., Chartas, G., Mori, K., & Pravdo, S. H. 2003, *ApJ*, 587, L51
- Vacca, W. D., & Sandell, G. 2011, *ArXiv e-prints*
- Walter, F. M., Bowyer, S., Linsky, J. L., & Garmire, G. 1980, *ApJ*, 236, L137
- Wang, J., Feigelson, E. D., Townsley, L. K., Broos, P. S., Román-Zúñiga, C. G., Lada, E., & Garmire, G. 2010, *ApJ*, 716, 474
- Wang, J., Townsley, L. K., Feigelson, E. D., Getman, K. V., Broos, P. S., Garmire, G. P., & Tsujimoto, M. 2007, *ApJS*, 168, 100
- Webb, R. A., Zuckerman, B., Platais, I., Patience, J., White, R. J., Schwartz, M. J., & McCarthy, C. 1999, *ApJ*, 512, L63
- Weisskopf, M. C., Brinkman, B., Canizares, C., Garmire, G., Murray, S., & Van Speybroeck, L. P. 2002, *PASP*, 114, 1
- White, R. J., & Basri, G. 2003, *ApJ*, 582, 1109
- Wiling, B. A., Greene, T. P., & Meyer, M. R. 1999, *AJ*, 117, 469

Zapatero Osorio, M. R., Martín, E. L., Bouy, H., Tata, R., Deshpande, R., & Wainscoat, R. J. 2006, ApJ, 647, 1405